Bulletin of the Seismological Society of America, Vol. 93, No. 2, pp. 882–890, April 2003

A Nearly Analytic Discrete Method for Acoustic and Elastic Wave Equations in Anisotropic Media

by Dinghui Yang, Jiwen Teng, Zhongjie Zhang, and Enru Liu

Abstract We transform the seismic wave equations in 2D inhomogeneous anisotropic media into a system of first-order partial differential equations with respect to time *t*. Based on the transformed equations, a new nearly analytic discrete method (NADM) is developed in this article. Our method enables wave propagation to be simulated in two dimensions through generally anisotropic and heterogeneous models. The space derivatives are calculated by using an interpolation approximation, while the time derivatives are replaced by a truncated Taylor expansion. Our analyses show that the error of the NADM is less than that of the conventional finite-difference method (FDM) and is about 1/60 to 1/100 of that of the FDM. We also demonstrate numerically that the stability of the NADM is higher than that of the FDM. The three-component seismic wave fields in two layered isotropic and transversely isotropic media (TIM) are simulated and compared with the conventional FDM. Again, we show from the three-component seismic wave fields that the NADM has higher accuracy, stronger stability, and less numerical dispersion, effectively suppressing the source noises as compared with the FDM.

Introduction

Different numerical methods have been developed and widely applied to solve the wave equations. Effective and accurate simulation of the three-component seismic wave field has become increasingly important for numerical investigation of seismic waves in complex and anisotropic media (Teng *et al.*, 1992). The numerical methods popularly used are: finite element (Chen, 1984), ray tracing (Červený, 1972; Červený and Firbas, 1984; Chapman and Shearer, 1989), reflectivity (Fuchs and Müller, 1971; Booth and Crampin, 1983a,b), finite difference (Kelly *et al.*, 1976; Igel *et al.*, 1995; Zhang *et al.*, 1993, 1999), and spectral element (Komatitsch and Vilotte, 1998). However, each method has its inherent advantages and disadvantages. The finite-element method requires large storage space, which makes it difficult to implement higher dimension or to compute large models. Using the ray-tracing method, we need to solve the geometrical motion parameters of reflective and transmissive waves at inner interfaces of a medium and cannot obtain full wave-field information. The reflectivity is only used media with homogeneous horizontal layers. The finite-difference method (FDM) for modeling seismic propagation is one of the most popular tools because of its rapidity and lesser storage. Unfortunately, when the wave equations are approximated by an explicit, standard finite-difference scheme, or when too-coarse computation grids are used, that is, when too few samples per wavelength are used, (Fei and Larner, 1995; Yang *et al.*, 2002), the discretization causes the phase speed to become a function of the discretization interval, resulting in undesirable ripples near large gradients in wave fields. The unphysical oscillations caused by discretization of the wave equation seriously affect our recognition of seismic propagation. Although the undesirable ripples can be suppressed using a flux-corrected transport (FCT) technique, initially developed by Book *et al.* (1975) and extended to anisotropic elastic wave propagation by Yang *et al.* (2002), the FCT method is unable to fully recover lost resolution by the numerical dispersion when the spatial sampling becomes too coarse (Fei and Larner, 1995; Yang *et al.*, 2002). Therefore, designing a new algorithm, which is different from the conventional methods mentioned previously, is very important for theoretical and practical applications.

In this article, we transform the 2D anisotropic wave equation into a system of first-order differential equations with respect to time *t*. On the basis of the transformed equations, we develop a new nearly analytic discretization method (NADM) using the Taylor series expansion and an interpolation method. In other words, the space derivatives are computed using an interpolation approximation and the time derivatives are replaced by a truncated Taylor series. As we will see in Analyses of Errors, the expression of wave displacements is in a nearly analytical form and the higher-order differential wave equation is used, which is different from the conventional methods using a discrete expression to approximate the original wave equation. We investigate

the error of the NADM using a 2D initial-value problem of plane-wave propagation. Three-component seismic wave fields in isotropic and transversely isotropic media (TIM) are simulated to test the NADM and to compare it with conventional FDM.

A Nearly Analytic Discrete Algorithm for the 2D Wave Equations

In this section, we design a new nearly analytic discretization algorithm to the 2D wave equation in inhomogeneous anisotropic media by using the Taylor expansion and interpolation method.

Basic Equations

In 3D anisotropic media, the wave equation is written as

$$\frac{\partial \sigma_{ij}}{\partial x_j} + f_i = \rho \frac{\partial^2 u_i}{\partial t^2} \tag{1}$$

where $\rho = \rho(x, y, z)$ is the density, u_i denotes the displacement component in the ith direction, f_i is the force-source component in the ith direction, and σ is the stress tensor. Stress and strain satisfy the following relationship (Hooke's law):

$$\sigma_{ij} = c_{ijkl}\, \varepsilon_{kl}$$

where c_{ijkl} is the fourth-order tensor of elastic constants and satisfies the following symmetry conditions:

$$c_{ijkl} = c_{jikl} = c_{ijlk} = c_{klij}$$

and subscripts i, j, k, and l take the values of 1, 2, and 3. ε corresponds to the strain tensor, and its elements can be expressed by

$$\varepsilon_{ij} = \frac{1}{2}\left(\frac{\partial u_i}{\partial x_j} + \frac{\partial u_j}{\partial x_i}\right)$$

Let $\partial u_i/\partial t = w_i$, $\partial w_i/\partial t = p_i$ then equation (1) can be rewritten as

$$\frac{\partial w_i}{\partial t} = \frac{1}{\rho}\left(\frac{\partial \sigma_{ij}}{\partial x_j} + f_i\right) = p_i \tag{2}$$

Let

$$U = \begin{bmatrix} u_x \\ u_z \\ u_y \end{bmatrix},\ W = \begin{bmatrix} w_x \\ w_z \\ w_y \end{bmatrix},\ P = \begin{bmatrix} p_x \\ p_z \\ p_y \end{bmatrix},\ F = \begin{bmatrix} f_x \\ f_z \\ f_y \end{bmatrix},$$

$$C_1 = \begin{bmatrix} c_{11} & c_{15} & c_{16} \\ c_{15} & c_{55} & c_{56} \\ c_{16} & c_{56} & c_{66} \end{bmatrix},\ C_2 = \begin{bmatrix} c_{15} & c_{13} & c_{14} \\ c_{55} & c_{35} & c_{45} \\ c_{56} & c_{36} & c_{46} \end{bmatrix},$$

$$C_3 = \begin{bmatrix} c_{15} & c_{55} & c_{56} \\ c_{13} & c_{35} & c_{36} \\ c_{14} & c_{45} & c_{46} \end{bmatrix},\ C_4 = \begin{bmatrix} c_{55} & c_{35} & c_{45} \\ c_{35} & c_{33} & c_{34} \\ c_{45} & c_{34} & c_{44} \end{bmatrix}$$

and partial differential operators:

$$L_1 = \frac{1}{\rho}\frac{\partial}{\partial x}\left(C_1 \frac{\partial}{\partial x} + C_2 \frac{\partial}{\partial z}\right),$$

$$\text{and}\quad L_2 = \frac{1}{\rho}\frac{\partial}{\partial z}\left(C_3 \frac{\partial}{\partial x} + C_4 \frac{\partial}{\partial z}\right)$$

then equation (2) in the 2D anisotropic case can be written as

$$\frac{\partial}{\partial t} W = (L_1 + L_2)U + \frac{1}{\rho} F = P \tag{3}$$

For computational purpose, we define the following vectors:

$$\overline{U} = \begin{bmatrix} U \\ \frac{\partial}{\partial x} U \\ \frac{\partial}{\partial z} U \end{bmatrix},\quad \overline{P} = \begin{bmatrix} P \\ \frac{\partial}{\partial x} P \\ \frac{\partial}{\partial z} P \end{bmatrix},\ \text{and}\ \overline{W} = \begin{bmatrix} W \\ \frac{\partial}{\partial x} W \\ \frac{\partial}{\partial z} W \end{bmatrix}$$

According to equation (3) and the definitions of W, $\bar{U}$, $\bar{P}$, and $\overline{W}$, we can obtain:

$$\frac{\partial^{m+k+l+1}\overline{U}}{\partial t^{m+1}\partial x^k \partial z^l} = \frac{\partial^{m+k+l}\overline{W}}{\partial t^m \partial x^k \partial z^l} = \frac{\partial^{m+k+l-1}\overline{P}}{\partial t^{m-1}\partial x^k \partial z^l} \tag{4}$$

where m, k, and l are nonnegative integers.

Nearly Analytic Discrete Method

Using the Taylor series expansion and equation (4), we can obtain the following analytical expressions for displacements:

$$\overline{U}_{i,j}^{n+1} = \overline{U}_{i,j}^{n} + \Delta t \overline{W}_{i,j}^{n} + \frac{(\Delta t)^2}{2}\overline{P}_{i,j}^{n} + \frac{(\Delta t)^3}{6}\left(\frac{\partial \overline{P}}{\partial t}\right)_{i,j}^{n} + \frac{(\Delta t)^4}{24}\left(\frac{\partial^2 \overline{P}}{\partial t^2}\right)_{i,j}^{n} \tag{5a}$$

and

$$\overline{W}_{i,j}^{n+1} = \overline{W}_{i,j}^{n} + \Delta t\overline{P}_{i,j}^{n} + \frac{(\Delta t)^2}{2}\left(\frac{\partial \overline{P}}{\partial t^2}\right)_{i,j}^{n} + \frac{(\Delta t)^3}{6}\left(\frac{\partial^2 \overline{P}}{\partial t^2}\right)_{i,j}^{n} \tag{5b}$$

where n is a nonnegative integer, (i,j) denotes a grid point, and Δt denotes the time increment. The expressions for $\bar{P}$, $\partial/\partial t(\bar{P})$, $\partial^2/\partial t^2(\bar{P})$, and their components $[\partial^2/\partial x^2(U)]_{i,j}^n$, $[\partial^2/\partial z^2(U)]_{i,j}^n$, $[\partial^2/\partial x\partial z(U)]_{i,j}^n$, etc. are listed in Appendices A and B.

Making use of equation (4), the partial derivatives of $\overline{W}$ with respect to x and z in equation (5) are calculated by the following approximate equation:

$$\left(\frac{\partial^{k+1}\overline{W}}{\partial x^k \partial z^l}\right)_{i,j}^{n} = \left[\left(\frac{\partial^{k+1}\overline{U}}{\partial x^k \partial z^l}\right)_{i,j}^{n} - \left(\frac{\partial^{k+1}\overline{U}}{\partial x^k \partial z^l}\right)_{i,j}^{n-1}\right] \Big/ \Delta t \tag{6}$$

where $2 \le k + l \le 3$.

Analyses of Errors

To investigate the accuracy of the NADM, we estimate the error and compare it with the FDM.

Theoretical Error

Using the Taylor series expansion, we find that the errors of $\partial^{m+l}U/\partial x^m z^l$ on $2 \le m + l \le 3$ and $4 \le m + l \le 5$ are, respectively, $O(h_1^4 + h_2^4)$ and $O(h_1^2 + h_2^2)$ (where $h_1 = \Delta x$, $h_2 = \Delta z$) caused by the interpolation approximation. The error of $\partial^{m+l+1}U/\partial t\partial x^m z^l$ $(2 \le m + l \le 3)$ is $O(\tau + h_1^4 + h_2^4)$ $(\tau = \Delta t)$ because of the use of equation (6) and the interpolation method. Therefore, we find that the error introduced by the NADM is in the order of $O(\tau^2 + h_1^4 + h_2^4)$ because of the use of equation (5) and the interpolation approximation, that is, the NADM is accurate fourth-order in space and second-order in time.

Numerical Error

To test the accuracy of numerical results, consider the following initial value problem:

$$\frac{\partial^2 u}{\partial x^2} + \frac{\partial^2 u}{\partial z^2} = \frac{1}{\alpha^2}\frac{\partial^2 u}{\partial t^2} \tag{7a}$$

$$u(0, x, z) = \cos\left(-\frac{2\pi f}{\alpha}\cdot\cos\theta_0\cdot x - \frac{2\pi f}{\alpha}\cdot\sin\theta_0\cdot z\right), \text{ and} \tag{7b}$$

$$\frac{\partial u(0, x, z)}{\partial t} = -2\pi f\cdot\sin\left(-\frac{2\pi f}{\alpha}\cdot\cos\theta_0\cdot x - \frac{2\pi f}{\alpha}\cdot\sin\theta_0\cdot z\right), \tag{7c}$$

where α is the velocity of the plane wave, f denotes the frequency, and θ_0 is an incident angle at time $t = 0$.

Obviously, the analytical solution for the initial problem (7) is

$$u(t, x, z) = \cos\left[2\pi f\left(t - \frac{x}{\alpha}\cos\theta_0 - \frac{z}{\alpha}\sin\theta_0\right)\right].$$

For simplicity, we choose $\Delta x = \Delta z = h$ and $\theta_0 = \pi/4$; the total grid numbers in the x and z directions are N. For comparison, we use the following FDM for equation (7a):

$$u_{i,j}^{n+1} = 2u_{i,j}^{n} - u_{i,j}^{n-1} + \left(\frac{\alpha\cdot\Delta t}{\Delta x}\right)^2\cdot(u_{i+1,j}^{n} - 2u_{i,j}^{n} + u_{i-1,j}^{n}) + \left(\frac{\alpha\cdot\Delta t}{\Delta z}\right)^2\cdot(u_{i,j+1}^{n} - 2u_{i,j}^{n} + u_{i,j-1}^{n}).$$

The root-mean-square (rms) deviation E from the analytical solution used for the quantitative measurement of the numerical accuracy is defined as

$$E = \left\{\frac{1}{N^2}\sum_{i=1}^{N}\sum_{j=1}^{N}[u_{i,j}^{n} - u(t_n, x_j, z_j)]^2\right\}^{1/2}$$

In our calculation, the time increment $\Delta t = (0.1\cdot\Delta x)/(\sqrt{2}\cdot\alpha)$ is chosen and the analytical solution is used on the artificial boundaries for the two methods (FDM and NADM). Different parameters listed in Table 1 are used for comparison of the errors and stability.

Figures 1, 2, and 3 show the computational results of E at different times for cases 1, 2, and 3, where two lines of E for the NADM (Δ) and the FDM ($\diamond$) are shown in a semilog scale. From Figures 1, 2, and 3 we find that the error introduced by the NADM measured by E is less than that of the FDM. In general, the error of the NADM is about 1/60 to 1/100 of that of the FDM at the same grid point. We also notice from Figure 3 that the accuracy can be improved by decreasing the spatial increment. For the time evolution, the error curve of the NADM tends to be smooth and steady, whereas the error of the FDM oscillates strongly (as seen in Figs. 2 and 3). The stability of the NADM is higher than that of the FDM.

Numerical Examples

Making use of the NADM, we simulate three-component seismic wave fields in 2D isotropic media and TIM, respectively. Figure 4 shows the model geometry. The computa-

Table 1
Calculating Parameters for Different Cases

Cases	α (m/sec)	f (Hz)	h (m)	N
1	4000	20	10	60
2	5000	25	10	60
3	4000	15	5	60

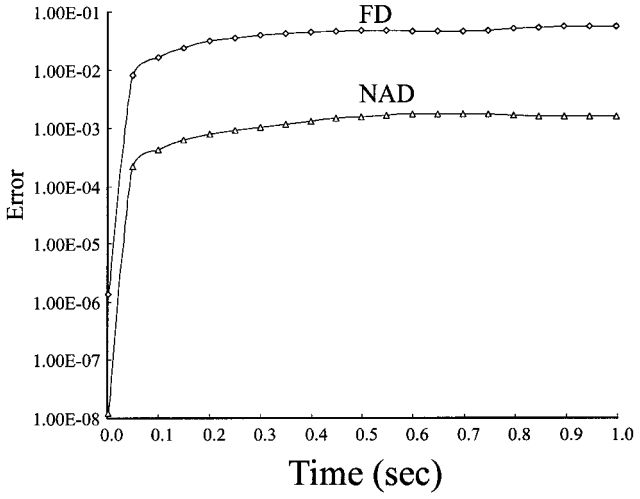

Figure 1. The errors of the NADM (Δ) and the FDM (◇) measured by E are shown in a semilog scale for case 1.

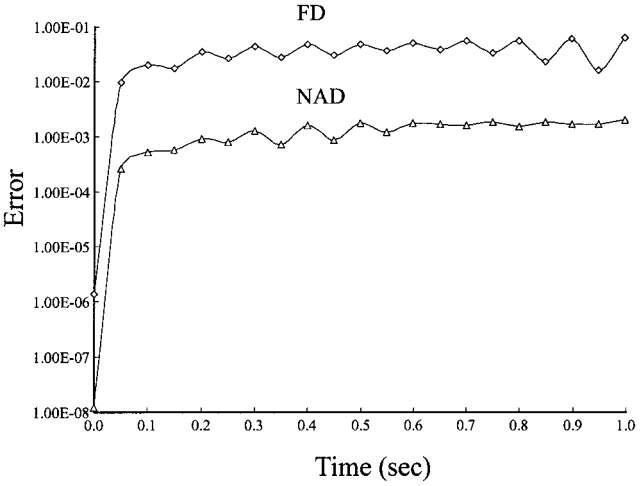

Figure 2. The errors of the NADM (Δ) and the FDM (◇) measured by E are shown in a semilog scale for case 2.

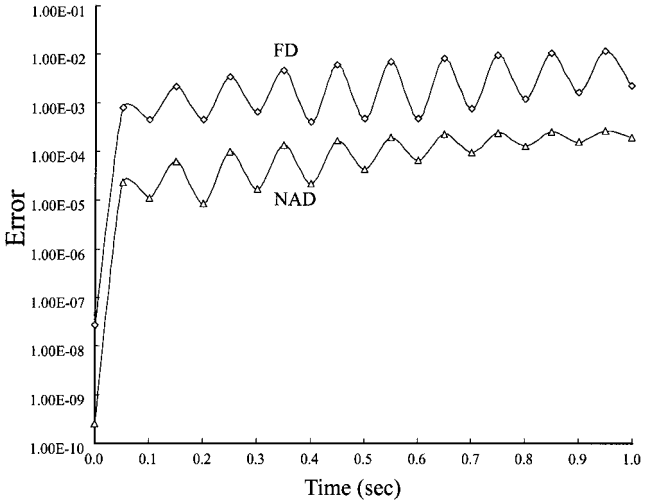

Figure 3. The errors of the NADM (Δ) and the FDM (◇) measured by E are shown in a semilog scale for case 3.

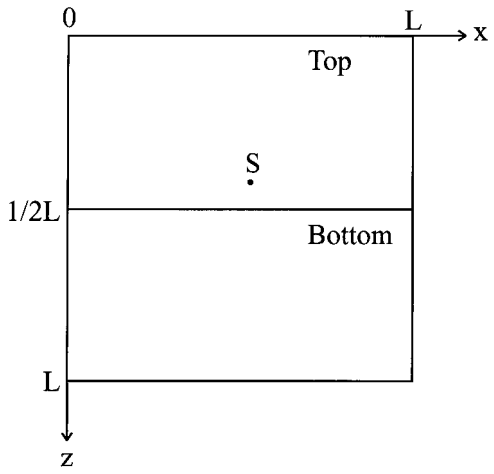

Figure 4. The model geometry. S denotes source.

tional region is $0 \le x \le L$, $0 \le z \le L$, and a horizontal discontinuity is located at $1/2L$. The source term is treated in the same way as Aboudi (1971) and Zahradnik *et al.* (1993) treated it, and the source has the following form:

$$f(t) = \sin(2\pi f_0 t)\exp(-4\pi^2 f_0^2 t^2/16)$$

with frequency $f_0 = 10$ Hz.

In 2D isotropic media and TIM with a vertical symmetry axis as presented in the following examples, antiplane *SH* waves and inplane *P-SV* waves are decoupled. In our examples presented subsequently, a line force polarized in the y direction is used to generate *SH* wave fields, and a line explosive source in the x–z plane is used to generate *P-SV* wave fields. However, for convenience of display, the three-component wave fields are given in the same figures (Figs. 5 to 8) as horizontal x-component *P-SV* waves, horizontal y-component *SH* waves, and vertical z-component *P-SV* waves.

Wave velocities vary with propagation directions in anisotropic media, so the stability condition $\Delta t \le 0.17h/\nu_{\max}$ obtained by numerical tests is chosen, where h corresponds to the spatial increment and $\nu_{\max}$ is the maximum qP velocity in the model. Of course, $0.17h/\nu_{\max}$ is not the upper limit of the interval for Δt, for which the NADM is stable, and the further theoretical stability condition will be given in a separate study.

Isotropic Model

In this model, S-wave and P-wave velocities are chosen to be $\beta = 1.196$ km/sec and $\alpha = 2.071$ km/sec, respectively, for the upper medium, and $\beta = 2.153$ km/sec and $\alpha = 3.729$

km/sec for the lower medium. The density is $\rho = 2.1$ g/cm^3. The number of grid points is 200 × 200, the model size is 3980 × 3980 ($L = 3980$ m), and the source is located at (x_s, z_s) = (1980 m, 1780 m). The spatial increments are $\Delta x = \Delta z = 20$ m, and the time increment is $\Delta t = 0.8 \times 10^{-3}$ sec.

Figure 5 shows the three-component snapshots at time $t = 0.56$ sec in the isotropic medium, where Figure 5b presents the wave-field snapshot of the u_y component, and Figures 5a,c show wave-field snapshots of horizontal and vertical components (u_x and u_z). Figure 5b clearly shows that the wavefront of the u_y-component snapshot (S wave in 2D isotropic medium) is a cycle at the inner interface. u_x- and u_z-component records are more complex, but we can also identify clearly the reflection, transmission, and the converted waves of P and SV waves at the horizontal interface (Fig. 5a,c). The computations to generate the results in Figure 5 were performed on a Pentium III 600 with 128 MB memory; this takes about 4.5 min.

TIM Model

Now we consider a two-layered TIM model. The elastic constants and densities that we use are $C_{11} = 14.2$, $C_{33} = 18$, $C_{13} = 5.4$, $C_{44} = 6.5$, $C_{66} = 3.8$, $\rho = 3.2$ g/cm^3, and $C'_{11} = 40.8$, $C'_{33} = 50.6$, $C'_{13} = 13.2$, $C'_{44} = 25$, $C'_{66} = 13.8$ $\rho' = 4.2$ g/cm^3 in the upper and lower layers, respectively (Fig. 4). The model size is 1990 × 1990 ($L = 1990$ m). The antiplane SH and inplane line explosion sources for P-SV waves are located at (x_s, z_s) = (950 m, 930 m). The spatial increments are $\Delta x = \Delta z = 10$ m and the time increment is $\Delta t = 0.2 \times 10^{-3}$ sec. The number of grid cells is also 200 × 200. The wave-field snapshots of components for u_x, u_y, and u_z at time 0.28 sec are given in Figure 6. Figure 6b shows that the wavefront of qSH wave is an

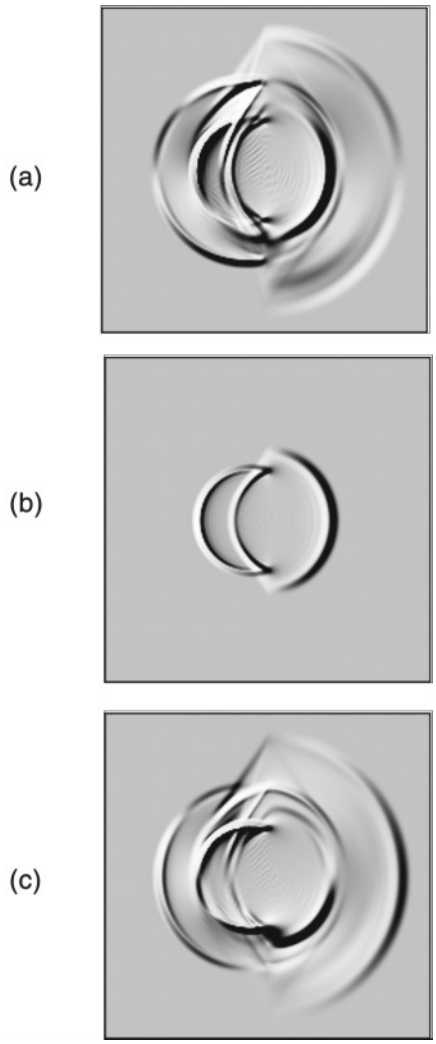

Figure 5. Snapshots of seismic wave fields for three components at time 0.56 sec in the two-layer isotropic medium, computed by the NADM, for (a) u_x component, (b) u_y component, and (c) u_z component.

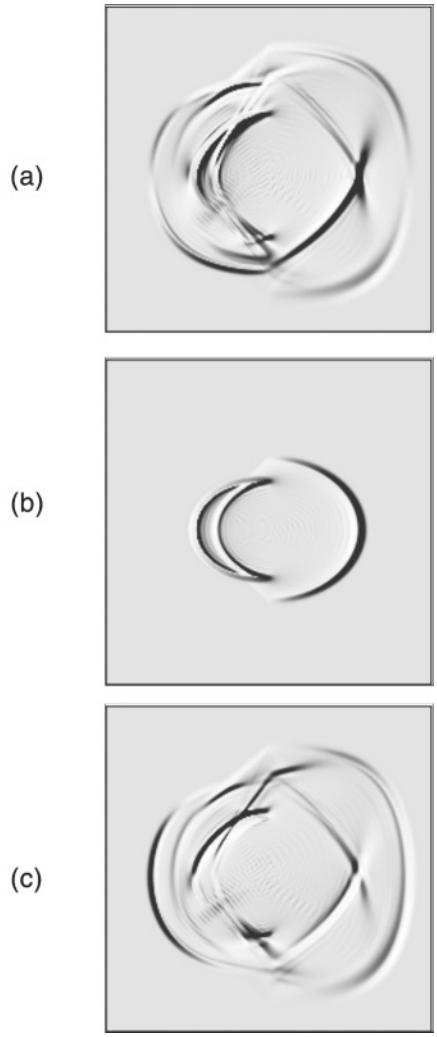

Figure 6. Snapshots of seismic wave fields for three components at time 0.28 sec in the two-layer transversely isotropic medium, computed by the NADM, for (a) u_x component, (b) u_y component, and (c) u_z component.

ellipse and the *qP* and *qSV* waves (Fig. 6a,c) show the directional dependence on propagation velocity. The *qSV* wavefronts can have cusps and triplications depending on the value of C_{13} (Faria and Stoffa, 1994). Triplications can be observed in the horizontal component *qSV* wavefronts (shown in Fig. 6a) and in the vertical component *qSV* wavefronts presented in Figure 6c. Moreover, we can also observe that the arrival times of *qSH* and *qSV* waves are different through comparing Figure 6b with Figures 6a,c.

To examine the validity of the NADM, we compare numerical results computed using the NADM and the conventional, second-order FDM. The model that we use is the same as that given previously in Figure 4, and the snapshots of seismic wave fields modeled by the FDM at time 0.28 sec are presented in Figure 7. We can see that the wavefronts of seismic waves simulated by two kinds of methods at the same time are identical (see Figs. 6 and 7). However, the snapshots in Figure 7 simulated by the FDM present stronger grid dispersion and source noise than the corresponding results in Figure 6 computed by the NADM.

To further test the dispersion error of the NADM, we choose a coarse spatial grid ($\Delta x = \Delta z = 50$ m) for the TIM model stated previously, the time interval $\Delta t = 2 \times 10^{-3}$ sec, and the model size is 9950×9950 ($L = 9950$ m) presented in Figure 4. The source is located at $(x_s, z_s) = (4750 \text{ m}, 4650 \text{ m})$. Wave-field snapshots of three displacement components simulated by the NADM at $t = 1.4$ sec are presented in Figure 8. Obviously, Figure 8 illustrates that the NADM has much less numerical dispersion and less noise even for the coarse grid without any additional treatments.

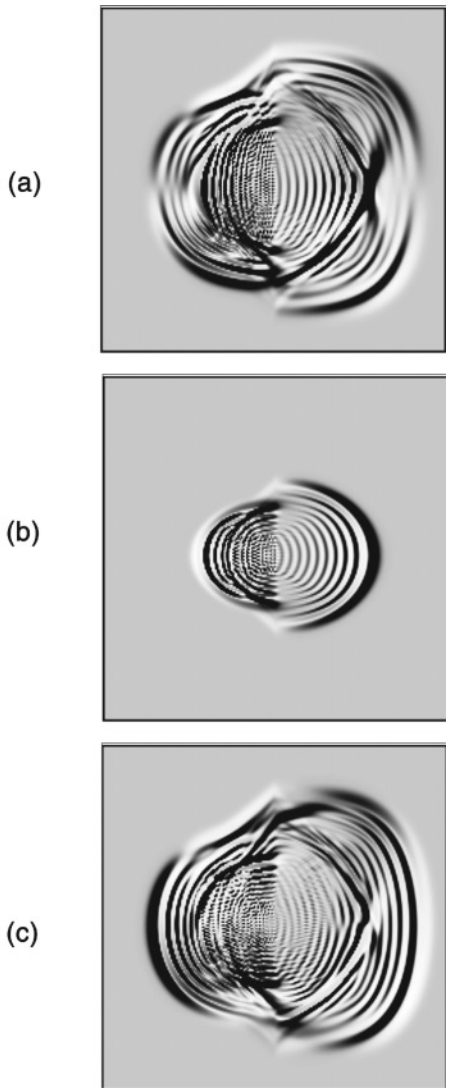

Figure 7. Snapshots of seismic wave fields for three components at time 0.28 sec in the two-layer transversely isotropic medium, computed by the conventional FCT, for (a) u_x component, (b) u_y component, and (c) u_z component.

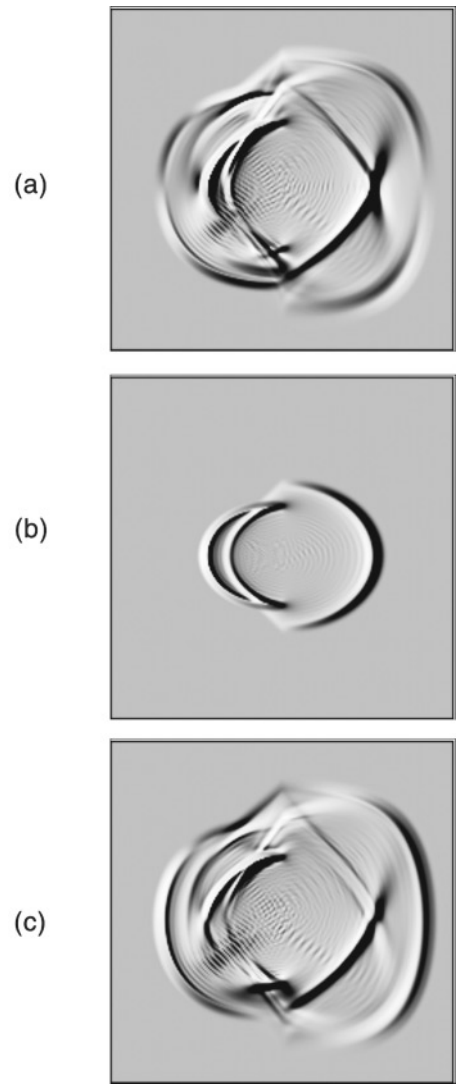

Figure 8. Wave-field snapshots for the coarse grid ($\Delta x = \Delta z = 50$ m) at time 1.4 sec in the two-layer transversely isotropic medium, computed by the NADM, for (a) u_x component, (b) u_y component, and (c) u_z component.

Note that the computations of generating Figures 6 and 7 were performed on a Pentium III 866 IBM PC with 128 MB memory. The iterating number of times is 1400, and it took about 8 min for the NADM and about 3 min for the conventional FDM. But when the time increment is chosen by $\Delta t = 0.4 \times 10^{-3}$ sec in terms of the stability given previously, it took about 4 min for the NADM, whereas the FDM suffers from strong numerical dispersion. On the same computer, it took about 4 min to generate Figure 8.

Discussion and Conclusions

The NADM is developed via the Taylor series expansion and the interpolation approximate method, that is, the time derivatives are approximated analytically by a truncated Taylor series and the space derivatives are calculated using the interpolation approximation. In addition, the higher-order differential wave equation compared with the original wave equation is used, which is different from the conventional calculation method using a discrete expression to approximate the original wave equation. When computing $U_{i,j}^{n+1}$, the NADM uses not only the values of the displacement U at the mesh point (i, j) and its neighboring grid points, but also the values of the partial derivatives of U with respect to time t and space x, z (see equation 5). The NADM retains more seismic information in both the function U^n and its partial derivatives. Furthermore the expression $U_{i,j}^{n+1}$ is very accurate. In fact, the error of the NADM is about 1/60 to 1/100 of that of the conventional FDM for the two models that we have presented. Introducing the local connection relations (Appendix B) greatly improves the continuity and derivability of the approximate function U^n (because U^n is an approximate variable during data processing) and furthermore stabilizes the NADM. Although the truncated Taylor series (equation 5a) also produces some errors because of losing the higher-order terms in the Taylor series, we can approximately incorporate the information of the higher-order terms from the additional 18 terms of $(\partial^{k+l}U/\partial x^k \partial z^l)_{i,j}^n$ $(2 \le k + l \le 5)$ by using the connection relations and introducing the interpolation function (see Appendix B). By doing this, we effectively suppress the loss of information included in the higher-order terms of the Taylor expansion, which therefore results in great accuracy and strong stability.

It appears that the CPU time of the NADM is more than that of the FDM, but in fact, because the NADM yields less numerical dispersion and has a higher stability than the FDM, we can afford to increase the time increment through adopting coarser spatial increments to achieve the same accuracy as that of the FDM on a finer grid with smaller time steps. Hence, the total CPU time of the NADM will not be larger than that of the FDM. Although the computational cost of the NADM is about 2.5 times of the conventional FDM, the computational speed of the NADM is about 10 times of the FDM on a fine grid to achieve the same accuracy as that of the NADM, and is about 80% of that of the FCT FDM (Yang *et al.*, 2002). But because the FCT algorithm uses an added diffusive treatment of smoothing displacement solutions, it cannot fully recover the resolution lost when the spatial sampling becomes too coarse (Fei and Larner, 1995), and the NADM does need not any additional treatments. In addition, the memory of the NADM depends mainly on storing values of $\bar{U}_{i,j}^n$, $\bar{W}_{i,j}^n$, and these partial derivatives $(\partial^{k+l}U/\partial x^k \partial z^l)_{i,j}^n$ $(2 \le k + l \le 3)$ and is basically identical with that of the FDM on a fine grid for obtaining the same accuracy, and the NADM does not need larger computer storage than the finite-element method, so it is suitable to compute large models.

From the examples presented in Figures 5, 6, and 8, we can see that the NADM can capture effectively the inner interface without any special treatments at the discontinuity; therefore, it can simulate seismic waves in complex geometries and heterogeneous anisotropic media without any additional treatments.

The NADM suppresses effectively the numerical dispersion caused by discretizing the wave equation by using the local interpolation compensation for the truncated Taylor series, whereas conventional finite-difference schemes to solve the wave equations suffer from numerical dispersion near large velocity contrast or when too few samples per wavelength are used. Our examples shown in Figures 6 and 8 also illustrate that the NADM causes less numerical dispersion without any additional treatments, whereas the standard FDM suffers from serious numerical dispersion as demonstrated in Figure 7. NADM allows us to use a coarse grid, that is, fewer samples per wavelength, to achieve the same accuracy in wave-field extrapolation and is similar to that obtained by conventional finite-difference methods on a fine grid or with an additional FCT correction. This is very important for programming and improving the accuracy in the computation of synthetic seismograms. Source noises occurring in numerical modeling are spurious oscillations or unphysical ripples. In wave-field simulations, the source noise lowers the resolution in the waveforms. Fortunately, the NADM can successfully suppress the noise caused by the seismic source located at grid points. Moreover, the computational cost of the NADM depends mainly on calculating these values of both $(\partial^{k+l}U/\partial x^k \partial z^l)_{i,j}^n$ $(2 \le k + l \le 5)$ and $(\partial^{k+l}\bar{W}/\partial x^k \partial z^l)_{i,j}^n$ $(2 \le k + l \le 3)$, and the computations of partial derivatives for different displacement components are decoupled and can be simultaneously computed. Therefore, further increases in efficiency are feasible through parallel computer programs so that the computations can be performed on multiple workstations or on a parallel computer.

Acknowledgments

This work was supported financially by the National Natural Sciences Foundation of China (Grant 40174012). We thank David Booth (British Geological Survey) and John Lovell for their comments, and Dr. Fred F. Pollitz (the editor), Dr. Stig Hestholm (reviewer), and another anonymous reviewer for their constructive comments, which significantly improve the readability of this article. Enru Liu was supported by the Edinburgh Anisotropy Project, and this article is published with the approval of the Executive Director of British Geological Survey.

References

Aboudi, J. (1971). Numerical simulation of seismic sources, *Geophysics* **36,** 810–821.

Book, D. C., J. P. Boris, and K. Hain (1975). Flux-corrected transport II: generalization of the method, *J. Comput. Phys.* **18,** 248–283.

Booth, D. C., and S. Crampin (1983a). The anisotropic reflectivity technique: theory, *Geophys. J. R. Astr. Soc.* **72,** 755–765.

Booth, D. C., and S. Crampin (1983b). The anisotropic reflectivity technique: anomalous arrives from an anisotropic upper mantle, *Geophys. J. R. Astr. Soc.* **72,** 767–782.

Červený, V. (1972). Seismic rays and ray intensities in inhomogeneous anisotropic media, *Geophys. J. R. Astr. Soc.* **29,** 1–33.

Červený, V., and P. Firbas (1984). Numerical modeling and inversion of travel-time of seismic body waves in inhomogeneous anisotropic media, *Geophys. J. R. Astr. Soc.* **76,** 41–51.

Chapman, C. H., and P. M. Shearer (1989). Ray tracing in azimuthally anisotropic media-II: quasi-shear-wave coupling, *Geophys. J.* **96,** 65–83.

Chen, K. H. (1984). Propagating numerical model of elastic wave in anisotropic inhomogeneous media—finite element method, *Symp. 54th SEG* **54,** 631–632.

Faria, E. L., and P. L. Stoffa (1994). Finite-difference modelling in transversely isotropic media, *Geophysics* **59,** 282–289.

Fei, T., and K. Larner (1995). Elimination of numerical dispersion in finite-difference modeling and migration by flux-corrected transport, *Geophysics* **60,** 1830–1842.

Fuchs, K., and G. Müller (1971). Computation of synthetic seismograms with the reflectivity method and comparison of observations, *Geophys. J. R. Astr. Soc.* **23,** 417–433.

Igel, H., Mora, P., and Riollet, B. (1995). Anisotropic wave propagation through finite-difference grids, *Geophysics* **60,** 1203–1216.

Kelly, K., R. Ward, S. Treitel, and R. Alford (1976). Synthetic seismograms: a finite-difference approach, *Geophysics* **41,** 2–27.

Komatitsch, D., and J.-P. Vilotte (1998). The Spectral Element method: an efficient tool to simulate the seismic response of 2D and 3D geological structures, *Bull. Seism. Soc. Am.* **88,** 368–392.

Teng, J. W., Z. J. Zhang, A. W. Wang, J. C. Wei, and L. X. Ji (1992). The study of anisotropy in elastic medium: Evolution, present situation and questions, *Chin. Prog. Geophys.* **7,** 14–28.

Yang, D. H., E. Liu, Z. J. Zhang, and J. Teng (2002). Finite-difference modelling in two-dimensional anisotropic media using a flux-corrected transport technique, *Geophys. J. Int.* **148,** 320–328.

Zahradnik, J., P. Moczo, and T. Hron (1993). Testing four elastic finite-difference schemes for behavior at discontinuities, *Bull. Seism. Soc. Am.* **83,** 107–129.

Zhang, Z. J., Q. D. He, and J. W. Teng (1993). The simulation of 3-component seismic records in 2D inhomogeneous transversely isotropic media, *Can. J. Explorational Geophys.* **29,** 51–58.

Zhang, Z. J., G. J. Wang, and J. M. Harris (1999). Multi-component wavefield simulation in viscous extensively dilatancy anisotropic media, *Phys. Earth Planet. Interiors* **114,** 25–38.

Appendix A: Computational Expressions for $\bar{P}$, $\partial/\partial t\bar{P}$, and $\partial^2/\partial t^2\bar{P}$

In terms of the definition, the vector $\bar{P}$, and the derivatives of $\bar{P}$ with respect to time are written as

$$\frac{\partial}{\partial t}\,\bar{P} \;=\; \left[\frac{\partial}{\partial t}\,P,\ \frac{\partial^2}{\partial t\partial x}\,P,\ \frac{\partial^2}{\partial t\partial z}\,P\right]$$

and

$$\frac{\partial^2}{\partial t^2}\,\bar{P} \;=\; \left[\frac{\partial^2}{\partial t^2}\,P,\ \frac{\partial^3}{\partial t^2\partial x}\,P,\ \frac{\partial^3}{\partial t^2\partial z}\,P\right]^T$$

where

$$\begin{aligned} P &= (L_1 + L_2)U + \frac{1}{\rho}\,F \\ \frac{\partial}{\partial t}\,P &= (L_1 + L_2)W + \frac{1}{\rho}\,\frac{\partial}{\partial t}\,F \\ \frac{\partial}{\partial x}\,P &= \frac{\partial}{\partial x}\,(L_1 + L_2)U + \frac{1}{\rho}\,\frac{\partial}{\partial x}\,F - \frac{F}{\rho^2}\,\frac{\partial\rho}{\partial x} \end{aligned}$$

and

$$\frac{\partial^2}{\partial t^2}\,P \;=\; (L_1 + L_2)^2U + (L_1 + L_2)\left(\frac{F}{\rho}\right) + \frac{1\partial^2 F}{\rho\,\partial t^2}$$

Similarly, we can easily obtain derivatives of $\partial^2P/\partial t\partial x$, $\partial^2P/\partial t\partial z$, $\partial^3P/\partial t^2\partial x$, and $\partial^3P/\partial t^2\partial z$, and the differential operators are given:

$$L_1 \;=\; \frac{1}{\rho}\,\frac{\partial}{\partial x}\left(C_1\,\frac{\partial}{\partial x} + C_2\,\frac{\partial}{\partial z}\right),\ L_2 \;=\; \frac{1}{\rho}\,\frac{\partial}{\partial z}\left(C_3\,\frac{\partial}{\partial x} + C_4\,\frac{\partial}{\partial z}\right).$$

Appendix B: Evaluation of the High-Order Partial Derivatives of the Displacement U

According to the Taylor series expansion on two variables, we define the interpolation function:

$$G(X,\ Z) \;=\; \sum_{r=0}^{M}\frac{1}{r!}\left(X\,\frac{\partial}{\partial x} + Z\,\frac{\partial}{\partial z}\right)^r U$$

then its partial derivatives with respect to x and z are

$$\begin{aligned} G_X(X,\ Z) &= \sum_{r=0}^{M-1}\frac{1}{r!}\left(X\,\frac{\partial}{\partial x} + Z\,\frac{\partial}{\partial z}\right)^r\frac{\partial}{\partial x}\,U \\ G_Z(X,\ Z) &= \sum_{r=0}^{M-1}\frac{1}{r!}\left((X\,\frac{\partial}{\partial x} + Z\,\frac{\partial}{\partial z}\right)^r\frac{\partial}{\partial z}\,U \end{aligned}$$

where M is an integer and can be determined in accordance with the designed method. In our study, we choose M 5 because the highest partial derivatives of the displacement U with respect to x and z in the computational formulae (5) and (6) are fifth-order.

To determine the values of the higher-order partial derivatives $(\partial^{k+l}U/\partial x^k\partial z^l)^n_{i,j}$ $(2 \le k + l \le 5)$ given in (5) and (6) by $U^n_{i+p,j+q}$, $(\partial U/\partial x)^n_{i+p,j+q}$, and $(\partial U/\partial z)^n_{i+p,j+q}$ $(p,\ q = -1,\ 0,\ 1)$. Let the function $G(x,\ z)$ satisfy the following interpolation conditions between the grid point $(i,\ j)$ and its eight neighboring nodes such as $(i - 1,\ j)$, $(i + 1,\ j)$, $(i,\ j - 1)$, $(i,\ j + 1)$, $(i - 1,\ j - 1)$, $(i - 1,\ j + 1)$, $(i + 1,\ j - 1)$, and $(i + 1,\ j + 1)$, as shown in Figure B1.

At the grid point $(i - 1,\ j)$:

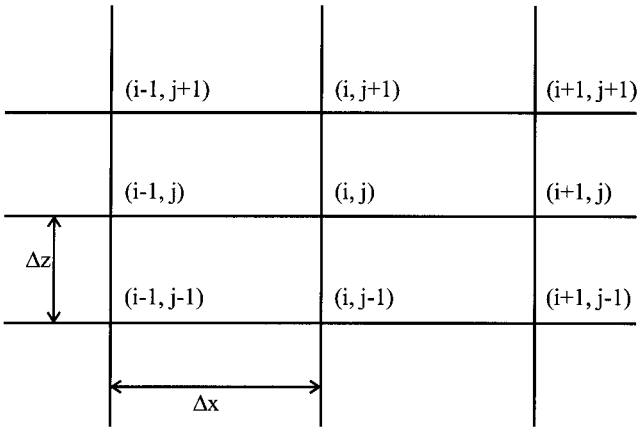

Figure B1. Local interpolation nodes.

$$[G(-\Delta x,0)]^n_{i,j} = U^n_{i-1,j}$$
$$[G_X(-\Delta x,0)]^n_{i,j} = \left(\frac{\partial}{\partial x}U\right)^n_{i-1,j}$$

and

$$[G_Z(-\Delta x,0)]^n_{i,j} = \left(\frac{\partial}{\partial z}U\right)^n_{i-1,j}$$

At the point $(i-1, j+1)$:

$$[G(-\Delta x, \Delta z)]^n_{i,j} = U^n_{i-1,j+1}$$
$$[G_X(-\Delta x, \Delta z)]^n_{i,j} = \left(\frac{\partial}{\partial x}U\right)^n_{i-1,j+1}$$

and

$$[G_Z(-\Delta x, \Delta z)]^n_{i,j} = \left(\frac{\partial}{\partial z}U\right)^n_{i-1,j+1}$$

Similarly, the other 18 connection relations at the nodes $(i-1, j-1)$, $(i, j+1)$, $(i, j-1)$, $(i+1, j+1)$, $(i+1, j)$, and $(i+1, j-1)$ can be easily written. Δx and Δz are the spatial increments in the x- and z-axis directions, respectively.

According to the interpolation relations given previously, we can obtain the high-order derivatives of U with respect to x and z as follows:

$$\left(\frac{\partial^2}{\partial x^2}U\right)^n_{i,j} = \frac{2}{(\Delta x)^2}(U^n_{i+1,j} - 2U^n_{i,j} + U^n_{i-1,j}) - \frac{1}{2\Delta x}\left[\left(\frac{\partial}{\partial x}U\right)^n_{i+1,j} - \left(\frac{\partial}{\partial x}U\right)^n_{i-1,j}\right],$$

$$\left(\frac{\partial^2}{\partial z^2}U\right)^n_{i,j} = \frac{2}{(\Delta z)^2}(U^n_{i,j+1} - 2U^n_{i,j} + U^n_{i,j-1}) - \frac{1}{2\Delta z}\left[\left(\frac{\partial}{\partial z}U\right)^n_{i,j+1} - \left(\frac{\partial}{\partial z}U\right)^n_{i,j-1}\right],$$

$$\left(\frac{\partial^2}{\partial x\partial z}U\right)^n_{i,j} = \frac{1}{2\Delta x}\left[\left(\frac{\partial}{\partial z}U\right)^n_{i+1,j} - \left(\frac{\partial}{\partial z}U\right)^n_{i-1,j}\right] + \frac{1}{2\Delta z}\left[\left(\frac{\partial}{\partial x}U\right)^n_{i,j+1} - \left(\frac{\partial}{\partial x}U\right)^n_{i,j-1}\right] - \left|\frac{1}{4\Delta x\Delta z}(U^n_{i+1,j+1} - U^n_{i+1,j-1} - U^n_{i-1,j+1} + U^n_{i-1,j-1}),\right.$$

$$\left(\frac{\partial^3}{\partial x^3}U\right)^n_{i,j} = \frac{15}{2(\Delta x)^3}(U^n_{i+1,j} - U^n_{i-1,j}) - \frac{3}{2(\Delta x)^2} \times \left[\left(\frac{\partial}{\partial x}U\right)^n_{i+1,j} + 8\left(\frac{\partial}{\partial x}U\right)^n_{i,j} + \left(\frac{\partial}{\partial x}U\right)^n_{i-1,j}\right]$$

$$\left(\frac{\partial^3 U}{\partial x\partial z^2}\right)^n_{i,j} = \frac{1}{2\Delta x\Delta z}\left[-\left(\frac{\partial U}{\partial z}\right)^n_{i+1,j+1} - \left(\frac{\partial U}{\partial z}\right)^n_{i-1,j-1} + \left(\frac{\partial U}{\partial z}\right)^n_{i,j+1} + \left(\frac{\partial U}{\partial z}\right)^n_{i,j-1} - 2\left(\frac{\partial U}{\partial z}\right)^n_{i+1,j} + 4\left(\frac{\partial U}{\partial z}\right)^n_{i,j} - 2\left(\frac{\partial U}{\partial z}\right)^n_{i-1,j}\right] + \frac{1}{(\Delta z)^2}\left[\left(\frac{\partial U}{\partial x}\right)^n_{i,j+1} - 2\left(\frac{\partial U}{\partial x}\right)^n_{i,j} + \left(\frac{\partial U}{\partial x}\right)^n_{i,j-1}\right] + \frac{1}{4\Delta x(\Delta z)^2}\left[5U^n_{i+1,j+1} - 5U^n_{i-1,j-1} - U^n_{i+1,j-1} + U^n_{i-1,j+1} - 4U^n_{i+1,j} + 4U^n_{i-1,j} - 6U^n_{i,j+1} + 6U^n_{i,j-1}\right],$$

where $U^n_{i,j}$, $(\partial U/\partial x)^n_{i,j}$, and $(\partial U/\partial z)^n_{i,j}$, denote $U(i\Delta x, j\Delta z, n\Delta t)$, $(\partial/\partial x)U(i\Delta x, j\Delta z, n\Delta t)$, and $(\partial/\partial z)U(i\Delta x, j\Delta z, n\Delta t)$.

Similarly, other expressions of $(\partial^{k+l}U/\partial x^k\partial z^l)^n_{i,j}$ $(2 \le k + l \le 5)$ can be obtained using the interpolation relations described previously.

Department of Mathematical Sciences
Tsinghua University
Beijing 100084, People's Republic of China
(D.Y.)

Institute of Geophysics
Chinese Academy of Sciences
Beijing 100101, People's Republic of China
(J.T., Z.Z.)

British Geological Survey
Murchison House
West Mains Road
Edinburgh, EH9 3LA, United Kingdom
(E.L.)

Manuscript received 23 May 2002.